# Supplemental materials

# Estimation of methane emissions from the U.S. ammonia fertilizer industry using a mobile sensing approach

Xiaochi Zhou[1,2], Fletcher H. Passow[1], Joseph Rudek[3], Joseph C. von Fisher[4], Steven P. Hamburg[3], John D. Albertson[1,*]

[1]School of Civil and Environmental Engineering, Cornell University, Ithaca, New York, United States

[2]Current address: California Air Resource Board, Sacramento, California, United States

[3]Environmental Defense Fund, New York, New York, United States

[4]Department of Biology, Colorado State University, Fort Collins, Colorado, United States

[*]Corresponding author: albertson@cornell.edu

# Contents

## S1. Data quality control

On 09/23/2016, the prevailing wind blew from the south. Downwind plume data were collected along a nearby road with an averaged sensor-to-facility distance ($x_s$) less than 100 m in Beatrice, NE. This data can be used to qualitatively identify the presence of natural gas (NG) emission from this plant. However, the small $x_s$ severely violated the point-source assumption and the associated uncertainty ($\sigma_e$) is too high (more details in Section S3), therefore, data collected on that day was not used for emission rate estimation.

The measured cross-plume integrated mixing ratios ($c_y$) on 09/13/2016 are more than an order or magnitude higher than that on 09/12/2016 (Figure S1), even though the GSV was driving on the same road in Verdigris, OK. The metrological conditions varied slightly when comparing data collected on 09/12/2016 to that on 09/13/2016 (e.g. mean wind velocity is 1.22 m/s on 09/13 versus 2.90 m/s on 09/12). However, this variation alone cannot explain the >10 times difference in $c_y$. A NG inspection vehicle operated by the state of Oklahoma was spotted near the Verdigris facility on 09/13/2016. It is suspected that a pipeline leak might have occurred and the data collected on 09/13/2016 was contaminated. Therefore, data collected in Verdigris, OK on the 09/13/2016 have been removed from the afterwards analysis.

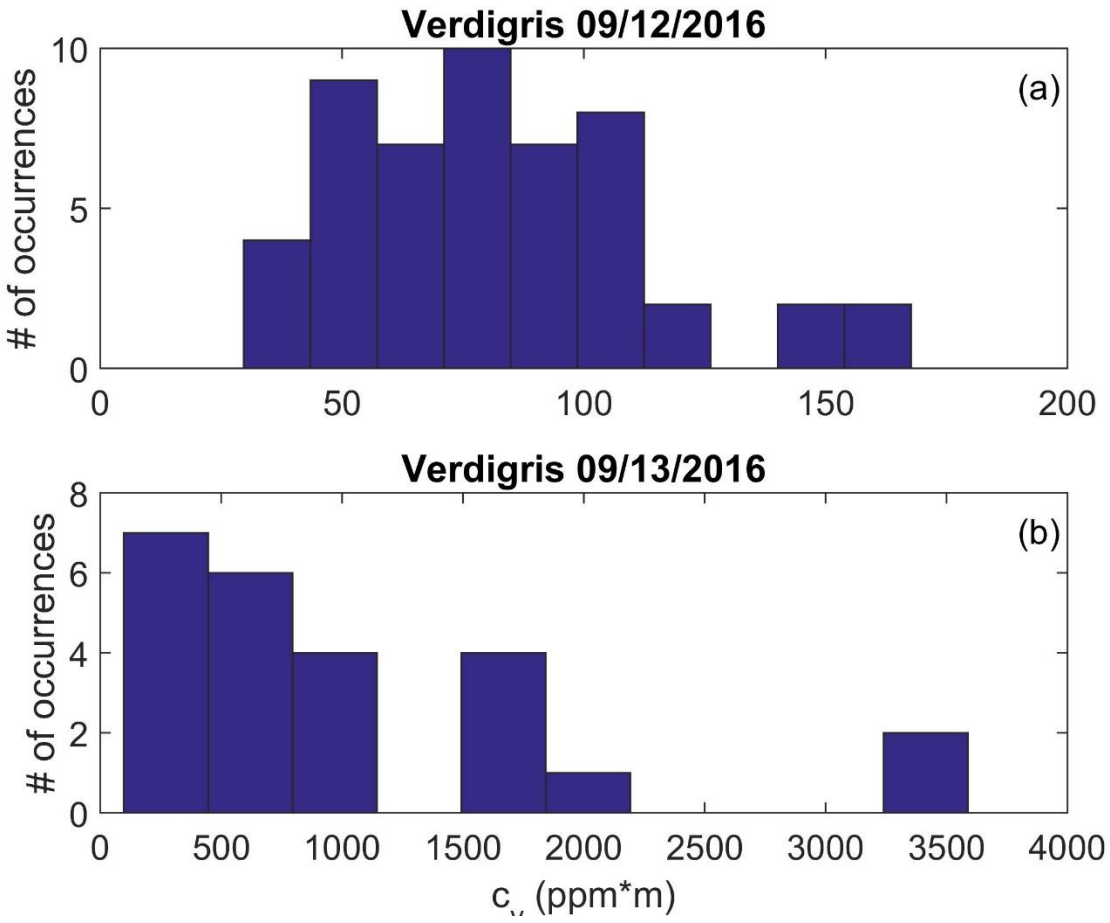


Figure S1. Histogram the cross-plume integrated mixing ratios ($c_y$) measured in Verdigris on (a) 09/12/2016 and (b) 09/13/2016 .

## S2. The determination of the error term in the likelihood function

The Bayesian inference requires an estimate of the total uncertainty, i.e. the "error term" ($\sigma_e$) in the likelihood function. According to Rao (2005)[1], total uncertainty in atmospheric dispersion modelling can be broadly classified as stochastic uncertainty, model errors, and data errors. The stochastic uncertainty comes from the stochastic nature of atmospheric plume dispersion, the model errors are related to the simplification of the model itself, and data errors are errors from the model input. Assuming that these uncertainties are uncorrelated and random, we can estimate the variance of the total uncertainty ($\sigma_e^2$) following Rao (2005)[1]:

$$\sigma_e^2 = \sigma_S^2 + \sigma_M^2 + \sigma_D^2 \quad \text{(S1)}$$

where $\sigma_S^2$, $\sigma_M^2$, $\sigma_D^2$ are the variance of the stochastic uncertainty, model errors, and data errors, respectively.

In this study, the stochastic uncertainty mainly comes from the fact that the cross-plume integrated methane mixing ratios ($c_y$) are closer to an instantaneous picture of the plume. Therefore, the variance of the stochastic uncertainty can be interpreted as the variability of the measured $c_y$:

$$\sigma_S^2 = \sigma^2(c_y) \quad \text{(S2)}$$

where $\sigma$ is the standard deviation operator.

Then, we evaluate the plume dispersion model errors, which can be described as the deviation of the model prediction (based on error-free input) from the measurements (excluding instrumentation error). After evaluating the plume dispersion model using independent data collected in Demark, Norway, and the U.S., it was found that the mean fractional error between the measured and modeled ensemble-averaged $c_y$ is -2%, and the standard deviation of the fractional error is 21%[2]. However, Hanna (1993)[3] pointed out that it's common for the same model to show a ±100% difference of performance when evaluated at different sites. After evaluating >20 air quality models, Chang and Hanna (2004)[4] conclude

that about ±20% mean bias and ±60% random scatter around the mean prediction represent the best achievable performance of air quality model. Meanwhile, they suggest that models with (1) mean bias within ±30% of the mean observations, (2) ~50% of model predictions are within a factor of two of the observations, and (3) all random scatters are within a factor of two to three of the mean observations, are considered as models with "good" performance. Given the great performance of the adopted model as shown in Gryning et al. (1967)[2], we considered it to be a "good" performance model, and assumed that a factor of two uncertainty to the mean observation to be a reasonable estimate (i.e. ~68% of model predictions are within a factor of two of the observations):

$$\sigma_M^2 = \left(2.0\overline{c_y}\right)^2 \quad \text{(S3)}$$

Finally, we evaluate the data errors of the dispersion model. All the input parameters for the dispersion model are listed in Table S1. We can further decompose it into errors from the meteorological parameters ($\sigma_W$), point-source assumption ($\sigma_X$), height of emission source ($\sigma_Z$), and methane analyzer ($\sigma_P$).

$$\sigma_D^2 = \sigma_W^2 + \sigma_X^2 + \sigma_P^2 \quad \text{(S4)}$$

Table S1. Parameters, sources, and the associated uncertainties for the plume dispersion model

| Parameter | Description (Unit) | Source | Error |
|---|---|---|---|
| $u_*$ | Friction velocity (m/s) | Estimated from 3D sonic anemometer | $\sigma_W$ |
| $L$ | Obukhov length (m) | Estimated from 3D sonic anemometer | $\sigma_W$ |
| $z_0$ | Surface roughness (cm) | Estimated from 3D sonic anemometer | $\sigma_W$ |
| $x_s$ | Plume travel distance (m) | Estimated from Google earth identified source location and MMP GPS location | $\sigma_X$ |
| $z_s$ | Height of emission source (m) | Assumed | $\sigma_X$ |
| $C$ | Methane mixing ratio (ppm) | Measured by MMP methane analyzer | $\sigma_P$ |
| $z_w$ | Height of 3D sonic anemometer (m) | Measured by on-site personnel | N/A |
| $z_m$ | Height of methane analyzer inlet (m) | Measured by on-site personnel | N/A |

Friction velocity ($u_*$) and Obukhov length ($L$) are both calculated directly from the 3D velocity and temperature measured at 10 Hz. Surface roughness ($z_0$) is estimated by inverting the logarithmic wind profile with stability correction. The estimated $z_0$ differs from site to site, and usually between 1cm to 5cm, which agrees well with the visual estimate of $z_0$ based on the landscape (tall grass). The estimated

$u_*$, $L$, and $z_0$ are then used to derive the plume advection speed ($\overline{U}$) and vertical dispersion coefficient ($D_z$). It was estimated that the uncertainty of estimating vertical profile of meteorological parameters (e.g. $\overline{U}$) for pollution dispersion modelling using wind statistics measured at one height has an uncertainty of 10% to 40% in daytime [5]. Similarly, Rao (2005) [1] suggested a 10-40% uncertainty in estimating lateral and vertical dispersion parameters. Considering the non-standard set-up of our 3D sonic anemometer and the relatively short measurement duration, we assume that the estimated $\overline{U}$ and $D_z$ both have an uncertainty of 40% in this study. Since both $\overline{U}$ and $D_z$ are linearly related with $c_y$ according to the dispersion model (i.e. $c_y^M(Q) = \frac{Q}{\overline{U}} D_z$, when the vehicle's path is perpendicular to the wind direction), we consider that they can both cause a 40% uncertainty of $c_y$. Note that the linear relation will not hold strictly if the vehicle's path is not perpendicular to the wind direction. However, the impact is minimal if the angle between them is not far from 90 degrees, which applies for most of our dataset. For simplicity, we estimate the error of meteorological parameters as the combined uncertainties from both $\overline{U}$ and $D_z$:

$$\sigma_W^2 = \left(0.4\overline{c_y}\right)^2 + \left(0.4\overline{c_y}\right)^2 \quad \text{(S5)}$$

Then, we analyze errors introduced due to the point-source assumption, which is related with the determination of the plume travel distance ($x_s$) and the height of emission source ($z_s$) in the dispersion model. The actual leak(s) may come from any NG-related equipment. Therefore, we assume that the actual leak(s) were located within a circle that covers most NG-related equipment of the plant (visual inspection from Google Earth). The radius of the circle ($x_D$), which defines the size of the area, varies from plant to plant with a range from ~100 to ~150 m. The point-source assumption allows us to attribute all emissions to a single, point-source emission located at the center of the circle. The actual height of the emission source is also unknown. Based on the point-source assumption, we consider $z_s$ to be 2 m, which is the average height of the main structure of the plants (around 4-5 m high). Since the plume maybe thermally buoyant, we allow $z_s$ to vary from ground level up to 10 m with an equal probability.

After defining the emission source, $x_s$ can be calculated as the Euclidean distance from the point-source to the center of the plume: $x_s = \|\mathbf{x}_0 - \mathbf{x}_c\|$, where $\mathbf{x}_0$ and $\mathbf{x}_c$ are the GPS coordinates of the point-source emission and the downwind plume center, respectively. For the $j^{th}$ mobile pass, we consider the plume center ($\mathbf{x}_c^j$) as the location where the peak methane concentration was observed along the pass. Given the instantaneous nature of the mobile sampling, $\mathbf{x}_c$ is estimated as the averaged $\mathbf{x}_c^j$ over sensor passes within a 30-minutes interval ($\mathbf{x}_c = \overline{\mathbf{x}_c^j}$) during which the mean wind direction is typically defined [6]. The uncertainty of $\mathbf{x}_c$ can be quantified as the standard deviation of $\mathbf{x}_c^j$ over sensor passes within a 30-minutes interval, i.e. $\sigma(\mathbf{x}_c^j)$. The A100 GPS unit (from Hemispheres GNSS, Scottsdale, AZ, USA) has a horizontal accuracy < 0.6 m with 95% confidence. This uncertainty is around two orders of magnitude smaller than $\sigma(\mathbf{x}_c^j)$, and therefore not considered in this study.

Based on the uncertainties of $\mathbf{x}_0$, $\mathbf{x}_c$, and $z_s$, we can estimate the uncertainty related with the point-source assumption as:

$$\sigma_X^2 = R_x \overline{c_y}$$
$$R_x = \frac{\sigma^2\left(c_y^M|_{\mathbf{x}_0', \mathbf{x}_c', z}\right)}{c_y^M|_{\mathbf{x}_0, \mathbf{x}_c, z_s}}, \text{where } \|\mathbf{x}_0' - \mathbf{x}_0\| \le x_D, \mathbf{x}_c' \sim N\left(\mathbf{x}_c, \sigma(\mathbf{x}_c^j)\right), z \in [0, 10] \quad \text{(S6)}$$

Equation (S6) is basically the lumped uncertainties of $\mathbf{x}_0$, $\mathbf{x}_c$, and $z_s$, by allowing them to vary independently within their own ranges. Since the actual emission rate ($Q$) is unknown, the denominator $c_y^M|_{\mathbf{x}_0, \mathbf{x}_c, z_s}$ is introduced to derive $R_x$, which can be understood as the uncertainty given a unit $c_y$. The complication of $\sigma^2\left(c_y^M|_{\mathbf{x}_0', \mathbf{x}_c', z}\right)$ only allows us to evaluate it numerically, therefore we adopted the bootstrapping method[7]. More specifically, $c_y^M|_{\mathbf{x}_0', \mathbf{x}_c', z}$ is calculated 100,000 times by randomly drawing $\mathbf{x}_0$, $\mathbf{x}_c$, and $z_s$ from their distributions, and $\sigma^2\left(c_y^M|_{\mathbf{x}_0', \mathbf{x}_c', z}\right)$ is the standard deviation of the calculated $c_y^M|_{\mathbf{x}_0', \mathbf{x}_c', z}$.

Here, we provide an example $R_x$ as a function $x_s$. As an example, we consider a surface roughness of 2 cm (typical for short grassland), under a typical meteorological condition (i.e. a friction velocity of 0.3 m/s and a neutrally stable atmospheric condition). Meanwhile, a typical value of 100 m and 50 m are considered for $x_D$ (uncertainty of the estimating the location of the point-source emission) and $\sigma(\mathrm{x}_c^j)$ (uncertainty of the estimating the downwind plume center), respectively. As shown in Figure S2, $R_x$ drops below 0.2 when $x_s$ is greater than ~400 m. This is applicable for most sampling conditions (Table. 1 in the main text), except for data conducted in Beatrice, NE on 09/23/2016, where $x_m$ is less than 100 m. Therefore, this particular data was excluded from the analysis due to excessive amount of error related to the point-source emission assumption. For other data, $\sigma_X^2$ will be evaluated case by case given different $x_s$ and meteoritical conditions.

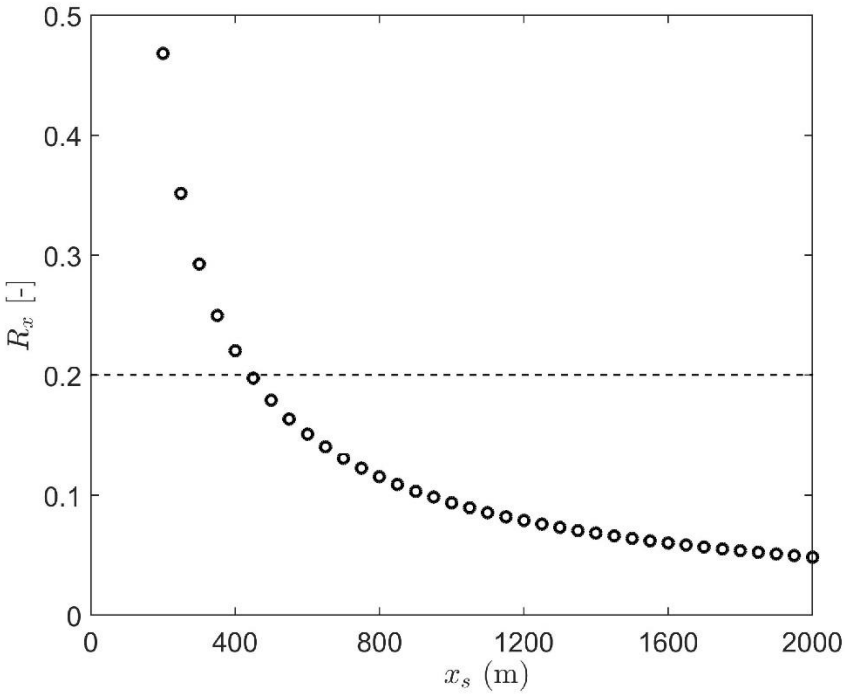


Figure S2. Uncertainty related with the point-source assumption given a unit $c_y$, $R_x$, plotted as a function of plume travel distance ($x_s$). Results are obtained with a surface roughness of 2 cm (typical for short grassland), under a typical meteorological condition (i.e. a friction velocity of 0.3 m/s and a neutrally stable atmospheric condition). Meanwhile, a typical value of 100 m and 50 m are considered for $x_D$ (uncertainty of the estimating the location of the point-source emission) and $\sigma(\mathrm{x}_c^j)$ (uncertainty of the estimating the downwind plume center), respectively.

142

143 Finally, we assess uncertainty from the methane analyzer onboard the GSV car ($\sigma_P$). The G2301
144 analyzer from Picarro Inc. [8] and the fast methane/ethane gas analyzer from Los Gatos Research Inc. [9]
145 show a rated sensor noise ($\sigma(C)$) of about 1 ppb and 2 ppb, respectively. Given the ppm level of ambient
146 methane concentration, $\sigma_P$ is only ~0.1%. Since $\sigma_P$ is around two orders of magnitude smaller than $\sigma_W^2$ or
147 $\sigma_X^2$, it is ignored in this study.

## S3. Natural gas throughput for U.S. NG-based ammonia fertilizer plants

Four plant-specific $E_N$ values are estimated from annual reports of some companies (Table S2), which are used to define the range of $E_N$ for plants whose $E_N$ are unknown. Worrell et al. (2000) reported an industrial-averaged $E_N$ of 39.3 GJ/Tg based on a survey of several U.S. ammonia fertilizer plants in 1999[10]. Based on an energy balance method similar as Equation (4) in the main text, Kermeli et al. (2017) estimated an industrial-averaged $E_N$ of 37.0 GJ/Tg for U.S. ammonia fertilizer plants in 2010[11]. The International Energy Agency (2007) reported an industrial-averaged $E_N$ of 37.9 TJ/Gg[12] based on industrial surveys. These reported industrial-averaged $E_N$ values all fall within the reported $E_N$ range from 34.7 to 40.0 GJ/Tg as shown in Table S2.

Table S2. A list of plant reported energy demand for ammonia production ($E_N$).

| Facility location | $E_N^P$ (GJ/Tg) |
|---|---|
| Donaldsonville, LA | 37.8[13] |
| Cherokee, AL | 38.7[14] |
| Pryor, OK | 34.7[14] |
| El Dorado, AR | 40.0[14] |

In 2015-2016, the capacity utilization rate ($R_c$) was reported from 0.54 to 1.06 by six plants[14-16], with an averaged $R_c$ of 0.82 and 0.88 for year 2015 and 2016, respectively (Table S3). Meanwhile, the United States Geological Survey (USGS) reported that ammonia plants in the U.S. operated at about 80% of their design capacity in 2015[17], which is fairly close to the averaged $R_c$ of those six facilities in 2015. Given the reported $R_c$ for the six plants, $R_c$ is considered to vary between 0.54 and 1.06 for the remaining plants whose $R_c$ are not publicly available.

Table S3. A list of facility reported $R_c$ values for 2015 and 2016.

| Facility location | $R_c$ (2015) | $R_c$ (2016) |
|---|---|---|
| Augusta, GA | 0.98[14, 16] | 0.86[16] |
| Cherokee, AL | 0.98[14] | 0.95[15] |
| El Dorado, AR | 0.54[14] | 0.65[15] |
| Geismar, LA | 0.98[16] | 1.06[16] |
| Lima, OH | 0.67[16] | 0.93[16] |
| Pryor, OK | 0.78[14] | 0.84[15] |

Using equation (4) of the main text, the NG throughput can be calculated for the nominal ($T_N$), best ($T_B$), and the worst ($T_W$) case, as detailed in the main text. The selected values of $E_N$ and $R_c$ are reported in Table S4, based on the reported $E_N$ and $R_c$ from some plants and industrial-averaged values. Note that the International Energy Agency reported $E_N$ value is adopted, since it is based on the most recent industrial survery.

Table S4. Selected value of $E_N$ and $R_c$ for the calculation of NG throughput for nominal, worst, and best case for NG-based ammonia fertilizer plants in the U.S. (2015-2016 scenario).

| Selected value | Nominal (expected NG throughput) | Worst (least NG throughput) | Best (most NG throughput) |
|---|---|---|---|
| $E_N$ (GJ/Tg) | 37.9[12] | 40.0[14] | 34.7[14] |
| $R_c$ (-) | 0.8[17] | 1.06[16] | 0.54[14] |

The gross production capacity of ammonia ($C_N$) and urea ($C_U$), and the estimated NG throughput under nominal ($T_N$), worst ($T_W$), and best ($T_B$) case for NG throughput of NG-based ammonia fertilizer plants in the U.S. are reported in Table S5 for the 2015-2016 scenario. Note that the El Dorado plant began production in 2016, therefore not included in the United States Geological Survey (USGS)' 2015 mineral yearbook[17]. Since $E_N$ and $R_c$ values are both reported for plants in Cherokee (AL), El Dorado (AR), and Pryor (OK) as shown in Table (S1) and Table (S2), $T_N$, $T_W$, and $T_B$ are the same for those plants.

Table S5. A list of gross ammonia production capacity ($C_N$), urea production capacity ($C_U$), and the estimated NG throughput under nominal ($T_N$), worst ($T_W$), and best ($T_B$) case for NG-based ammonia fertilizer plants in the U.S. for 2015-2016 scenario.

| Location | $C_N$ [Gg/yr] | $C_U$ [Gg/yr] | $T_N$ [Gg/yr] | $T_W$ [Gg/yr] | $T_B$ [Gg/yr] |
|---|---|---|---|---|---|
| Augusta, GA | 800[16] | 500[16] | 522 | 550 | 480 |
| Beatrice, NE | 265[17] | 57[18] | 156 | 218 | 97 |
| Beaumont, TX | 331[19] | 0[18] | 192 | 269 | 119 |
| Borger, TX | 451[20] | 92[18] | 266 | 371 | 164 |
| Cherokee, AL | 163[15] | 85[18] | 119 | 119 | 119 |
| Cheyenne, WY | 178[17] | 111[18] | 108 | 151 | 67 |
| Creston, IA | 32[17] | 0[18] | 19 | 26 | 11 |
| Dodge City, KS | 280[17] | 72[18] | 166 | 231 | 103 |
| Donaldsonville, LA | 3,933[13] | 3,546[18] | 2,430 | 3,219 | 1,640 |
| East Dubuque, IL | 337[17] | 141[18] | 202 | 282 | 125 |
| El Dorado, AR | 408[15] | 0[18] | 203 | 203 | 203 |
| Enid, OK | 930[17] | 485[18] | 561 | 783 | 348 |
| Faustina, LA | 500[21] | 0[18] | 290 | 406 | 179 |
| Fort Dodge, IA | 350[17] | 152[18] | 210 | 293 | 130 |
| Geismar, LA | 500[16] | 0[16] | 385 | 406 | 352 |
| Hopewell, VA | 590[22] | 0[18] | 343 | 479 | 212 |
| Lima, OH | 700[16] | 400[16] | 492 | 519 | 452 |
| Port Neal, IA | 1,116[13] | 328[18] | 662 | 925 | 410 |
| Pryor, OK | 213[15] | 137[18] | 125 | 125 | 125 |
| St Helens, OR | 101[17] | 104[18] | 63 | 88 | 39 |
| Verdigris, OK | 1,098[13] | 646[18] | 665 | 928 | 413 |
| Woodward, OK | 435[13] | 293[18] | 265 | 370 | 165 |
| Yazoo City, MS | 517[13] | 174[18] | 308 | 430 | 191 |

## References


1. Rao, K. S., Uncertainty analysis in atmospheric dispersion modeling. *Pure and applied geophysics* **2005,** *162*, (10), 1893-1917.
2. Gryning, S.-E.; Holtslag, A.; Irwin, J. S.; Sivertsen, B., Applied dispersion modelling based on meteorological scaling parameters. *Atmospheric Environment (1967)* **1987,** *21*, (1), 79-89.
3. Hanna, S., Uncertainties in air quality model predictions. In *Transport and Diffusion in Turbulent Fields*, Springer: 1993; pp 3-20.
4. Chang, J. C.; Hanna, S. R., Air quality model performance evaluation. *Meteorology and Atmospheric Physics* **2004,** *87*, (1-3), 167-196.
5. Wilczak, J. M.; Phillips, M. S., An indirect estimation of convective boundary layer structure for use in pollution dispersion models. *Journal of climate and applied meteorology* **1986,** *25*, (11), 1609-1624.
6. Stull, R. B., *An introduction to boundary layer meteorology*. Springer Science & Business Media: 2012; Vol. 13.
7. Mooney, C. Z.; Duval, R. D.; Duvall, R., *Bootstrapping: A nonparametric approach to statistical inference*. Sage: 1993.
8. Picarro Inc. CRDS Analyzer for CO2/CH4/H2O in Air - Model G2301. http://www.picarro.com/assets/docs/CO2_CH4_H2O_in_Air.pdf (04/18/2019),
9. Los Gatos Research Inc. Fast methane/ethane gas analyzer (CH4, C2H6). http://www.lgrinc.com/analyzers/overview.php?prodid=42&type=gas (04/18/2019),
10. Worrell, E.; Phylipsen, D.; Einstein, D.; Martin, N. Energy use and energy intensity of the US chemical industry. https://www.osti.gov/servlets/purl/773773 (04/18/2019),
11. Kermeli, A.; Worrell, E.; Graus, W.; Corsten, M. Energy Efficiency and Cost Saving Opportunities for Ammonia and Nitrogenous Fertilizer Production-An ENERGY STAR® Guide for Energy and Plant Managers. https://www.energystar.gov/sites/default/files/tools/Fertilizer_guide_170418_508.pdf (04/18/2019),
12. International Energy Agency Tracking Industrial Energy Efficiency and CO2 Emissions. https://www.iea.org/publications/freepublications/publication/tracking_emissions.pdf (04/18/2019),
13. CF Industries Holdings Inc. CF Industries 2016 Annual Report. https://www.snl.com/IRW/FinancialDocs/4533245 (04/18/2019),
14. LSB Industries Inc. LSB Industries 2015 Annual Report. http://investors.lsbindustries.com/phoenix.zhtml?c=114410&p=irol-reportsAnnual (04/19/2019),
15. LSB Industries Inc. LSB Industries 2016 Annual Report. http://investors.lsbindustries.com/phoenix.zhtml?c=114410&p=irol-reportsAnnual (04/19/2019),
16. Potash Corporation of Saskatchewan Inc. PotashCorp 2016 Annual Report. https://www.nutrien.com/sites/default/files/uploads/2017-07/POT_2016_AIR_Full_Report.pdf (04/19/2019),
17. United States Geological Survey 2016 Minerals Yearbook, nitrogen (advanced release). https://minerals.usgs.gov/minerals/pubs/commodity/nitrogen/myb1-2016-nitro.pdf (04/18/2019),
18. International Fertilizer Industry Association World Ammonia Capacities. https://www.ifastat.org/ (04/18/2019),
19. OCI N. V. Annual report 2016. http://www.oci.nl/investor-relations/financial-reports/ (04/19/2019),
20. Agrium Inc. Agrium 2016 Annual Report. https://www.nutrien.com/sites/default/files/uploads/2017-07/2016_annual_report_-_final_0.pdf (04/18/2019),
21. The Mosaic Company 2016 annual report. http://investors.mosaicco.com/GenPage.aspx?IID=4097833&GKP=209119 (04/18/2019),
22. AdvanSix Inc. 2016 annual report. http://investors.advansix.com/sec-filings/annual-reports-and-proxy-materials (04/18/2019),